

# Electric Field Induced Biomimetic Transmembrane Electron Transport Using Carbon Nanotube Porins

Jacqueline M. Hicks, Yun-Chiao Yao, Sydney Barber, Nigel Neate, Julie A. Watts, Aleksandr Noy, and Frankie J. Rawson\*

Cells modulate their homeostasis through the control of redox reactions via transmembrane electron transport systems. These are largely mediated via oxidoreductase enzymes. Their use in biology has been linked to a host of systems including reprogramming for energy requirements in cancer. Consequently, the ability to modulate membrane redox systems may give rise to opportunities to modulate underlying biology. The current work aims to develop a wireless bipolar electrochemical approach to form on-demand electron transfer across biological membranes. To achieve this goal, it is shown that by using membrane inserted carbon nanotube porins (CNTPs) that can act as bipolar nanoelectrodes, one can control electron flow with externally applied electric fields across membranes. Before this work, bipolar electrochemistry has been thought to require high applied voltages not compatible with biological systems. It is shown that bipolar electrochemical reaction via gold reduction at the nanotubes can be modulated at low cell-friendly voltages, providing an opportunity to use bipolar electrodes to control electron flux across membranes. The authors provide new mechanistic insight into this newly describe phenomena at the nanoscale. The results presented give rise to a new method using CNTPs to modulate cell behavior via wireless control of membrane electron transfer.


occurring electrochemical mediators which facilitate electron transfer<sup>[2]</sup> and are present in all forms of life.<sup>[3]</sup> They are vitally important in cellular defense,<sup>[3,4]</sup> redox homeostasis, maintaining cellular energy levels, and autophagy.<sup>[5]</sup> An ubiquitous example of a TP MET and one of the most well-studied is the nicotinamide adenine dinucleotide phosphate oxidase (NOX) reductase family. Present in almost all cell types, NOX is involved in signaling and DNA regulation and is vital for maintaining the redox state of the cell. Unsurprisingly, malfunctioning NOX has been linked to numerous diseases and pathologies<sup>[6]</sup> including neurodegenerative diseases and dementia.<sup>[7]</sup> Therefore, if we can devise techniques to artificially transport free electrons across biological membranes, it would open up new opportunities to modulate cell biology in the future. For example, if we can alter membrane electron transfer we have the opportunity to reprogram cellular metabolism to restore cells' electrical communication to a normal state which, may be useful in developing new bioelectronic medicines.<sup>[8,9]</sup>

Voltage-dependent anion-selective channels (VDACS)<sup>[5]</sup> are a subset of the TP MET family that act as switchable porins within the membrane for the transport of anions and have been shown to transfer electrons via redox, activated by a change in potential.

## 1. Introduction

Trans-plasma membrane electron transport systems (TPMETs) are a ubiquitous family of proteins that facilitate the transport of electrons across membranes through redox cascades.<sup>[1]</sup> TPMETs consist of enzymes alone or in combination with naturally

Dr. J. M. Hicks, Dr. J. A. Watts, Dr. F. J. Rawson  
Biodiscovery Institute  
School of Pharmacy  
Division of Regenerative Medicine and Cellular Therapies  
University of Nottingham  
Nottingham NG7 2RD, UK  
E-mail: frankie.rawson@nottingham.ac.uk

 The ORCID identification number(s) for the author(s) of this article can be found under <https://doi.org/10.1002/sml.202102517>.

© 2021 The Authors. Small published by Wiley-VCH GmbH. This is an open access article under the terms of the Creative Commons Attribution License, which permits use, distribution and reproduction in any medium, provided the original work is properly cited.

DOI: 10.1002/sml.202102517

Dr. Y.-C. Yao, A. Noy  
School of Natural Sciences  
University of California Merced  
Merced 95343, USA  
Dr. Y.-C. Yao, S. Barber, Prof. A. Noy  
Materials Science Division  
Lawrence Livermore National Laboratory  
Livermore 94550, USA  
S. Barber  
United States Naval Academy  
Annapolis 21402, USA  
Dr. N. Neate  
Nanoscale and Microscale Research Centre  
University of Nottingham  
Nottingham NG7 2RD, UK

VDACs are present in the plasma membrane in numerous cell types<sup>[10]</sup> including neurons,<sup>[11]</sup> remaining inactive until a change in the membrane potential is detected.<sup>[12]</sup> The need for VDACs to be “activated” and have their pores opened explains how they are non-lethal, although the VDACs are thought to be involved in both ATP release and volume control<sup>[13]</sup> of the cytosol playing a regulatory role in apoptosis. VDACs and TPMETs are upregulated in various cancers;<sup>[14]</sup> and are involved in cancer development and progression.<sup>[15]</sup> VDACs have also been shown to play a role in apoptosis within differentiated neurons<sup>[16]</sup> and to be involved in amyloid beta toxicity in certain disease states including Alzheimers.<sup>[11]</sup> Designing biomimetic VDACs whose function can be controlled by external stimulus would be a key step in the treatment of such diseases.

The design and use of biomimetic membrane proteins (BMPs), including artificial TPMETs and VDACs, has drawn a lot of attention over the last decade.<sup>[17]</sup> The attraction of BMPs is twofold: first, they can be used for individual cellular measurements such as membrane potential and have proven to be extremely useful in optogenetics<sup>[18]</sup> where light is used to manipulate ion channels for precise activation or inhibition of neuronal signals. Second, BMPs may be used in electrochemical therapies and not only for the detection of aberrant cellular behavior but also in its correction.<sup>[19]</sup> BMPs were recently shown by Ma et al. to be capable of correcting malfunctioning cells by injecting nanoparticles into mice, where those nanoparticles were able to bind to retinol photoreceptors and convert near IR light into the visible spectrum, restoring sight.<sup>[20]</sup> Nanoparticles and nanotubes are common building block BMPs.<sup>[21]</sup> However, for them to be useful they need to be functionalized to be water-soluble, active within biological media,<sup>[22]</sup> and able to be amphiphilic so they can insert and remain within the plasma membrane. These goals have been achieved with several approaches including protein cage,<sup>[23]</sup> DNA origami,<sup>[24]</sup> and the attachment of ligands.<sup>[25]</sup>

An emerging BMP type-carbon nanotube porins (CNTPs) are artificial porins based on lipid-coated ultrashort carbon nanotubes (CNTs) that can self-insert into membranes.<sup>[25]</sup> They are similar in size to VDACs<sup>[26]</sup> with diameters ranging from 0.7–1.5 nm and with a concentration of charged groups at either terminus making the narrow 0.7 nm CNTPs appear “closed,” like VDACs, under normal biological conditions. Besides their ability to act as a channel for charged particles or water transport,<sup>[27]</sup> CNTPs are conductive<sup>[28]</sup> and potentially could act as wireless bipolar electrodes (BPEs). BPEs, placed within an electric field are polarized allowing for the reduction or oxidation of molecules at either terminus;<sup>[29,30]</sup> similar to how TPMETs/VDACs reduce oxidants extracellularly while oxidizing reductants intracellularly. Typically, the potential experienced at the BPE will be a fraction of the potential applied across the two driving electrodes, dependent on the ratio between the length of the BPE and the distance between the driving electrodes.<sup>[31]</sup> Previously to induce bipolar electrochemistry at CNTs that were millimetres in length an applied voltage in the kV region was used.<sup>[30]</sup> Such a drastic potential drop would not be useable in biological systems. However, recently it has been shown that nano-BPEs that do not obey these rules and can function with much lower driving potentials can be used.<sup>[32]</sup> This is because earlier research has failed to take account of capacitance

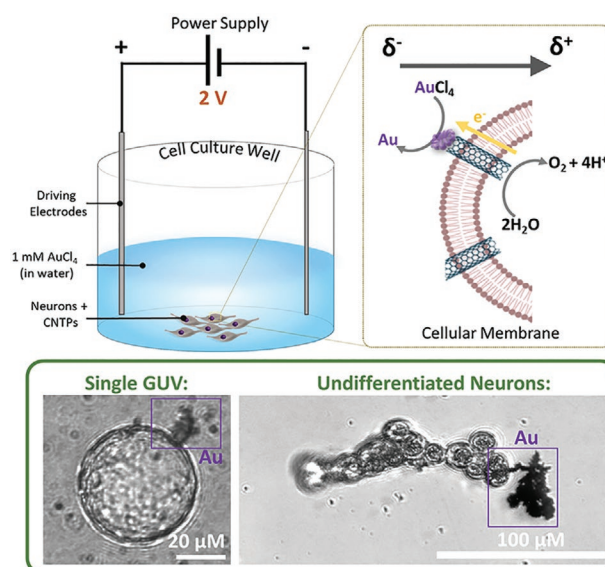


**Figure 1.** Summary schematic showing the experimental setup within a cell culture well of the driving electrodes and their placement on either side of the growth of NG108-15 undifferentiated neurons. CNTPs within neuronal membranes were polarized triggering the reduction of gold chloride to solid gold deposits on the CNTP terminus. Brightfield images below show this deposition on both a giant unilamellar vesicle (GUV) and the neurons.

increase at structures below 50 nm<sup>[33]</sup> and the enhanced electric field around the nanoscale conductive objects

Herein, we describe a nanotechnology-based route for controlling membrane electron transport. To investigate the use of CNTPs as BPEs and as artificial VDACs within biological systems (**Figure 1**), CNTPs were self-inserted into giant unilamellar vesicles (GUVs) which act as a simplified cellular model<sup>[34]</sup> and can be studied using normal cell biology techniques.<sup>[35]</sup> GUVs were essential in the study of the function of CNTPs as nano-BPEs without the presence of native VDACs or other membrane proteins that may obscure results. After the initial studies in GUVs to ascertain the key parameters it was possible to investigate the CNTPs within a complex cellular system. Studies with a neuronal cell line (NG108-15) showed that CNTPs embedded within biological membranes can act as bipolar wireless electrodes and control localized redox events at cell-friendly voltages.

## 2. Results and Discussion

We have inserted CNTPs into GUVs by adding lipid-coated CNTPs to the lipid mixture during the GUV preparation step. Before the incorporation of the CNTPs into GUVs, they were modified with the FITC-based fluorophore, 6-aminofluorescein (6AF), via 1-ethyl-3-(3-dimethylaminopropyl) carbodiimide hydrochloride (EDC)/N-hydroxysuccinimide (NHS) carbodiimide coupling chemistry, to enable us to track the location of the CNTPs (see **Figure 2**). To separate modified CNTPs the solution was passed through a sepharose gel column (CL-6B) to separate particles by size with fractional components identified by their absorption profiles (see **Figure 2D**). The covalent binding of the CNTPs to the 6AF fluorophore was then confirmed by FTIR and Raman spectroscopy (see Supporting Information).

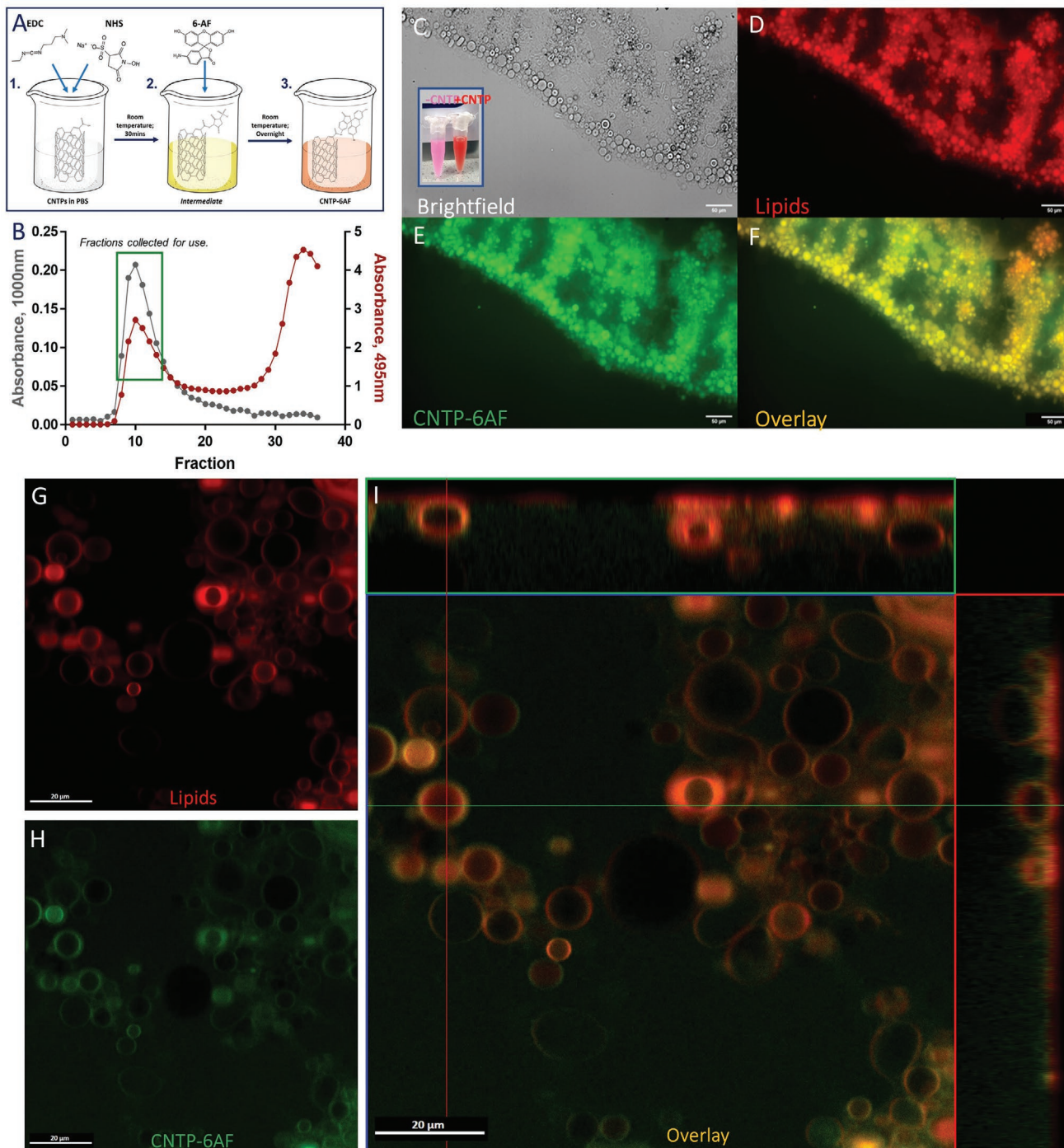


**Figure 2.** A,B) Modification of CNTPs with 6-aminofluorescein (6AF). A) Schematic of the reaction of CNTPs with 6AF via EDC/NHS chemistry. Step 1: solubilization of CNTPs with EDC (80 mM) and NHS (20 mM) which is left to react at room temperature for 30 minutes. Step 2: Addition of 6AF (final concentration 2.5 mM) which forms a yellow solution and is left overnight to react in the dark at room temperature. Step 3: Final product forms an orange solution. B) After separation of the product by size, gel-chromatography fractions absorbance is measured at 1000 nm (left axis, CNTPs) and 495 nm (right axis, 6AF). C) Brightfield microscopy of GUVs formed from rehydration. Inset Image- Shows difference in solution colors of the 18:1 Liss Rhod PE GUVs with and without the CNTP-6AF. D) Fluorescence microscopy of GUVs made with 18:1 Liss Rhod PE and CNTP-6AF. Excitation/emission: 560/583 nm, shows the 18:1 Liss Rhod PE lipid content of the GUVs. E) Excitation/emission: 490/520 nm, from the CNTP-6AF fluorophore. F) Overlay of the red and green channels. Scale bars are 50  $\mu\text{m}$ . G–I) Confocal microscopy of GUVs made with 18:1 Liss Rhod PE and CNTP-6AF. G) Excitation/emission: 561/624 nm, shows the 18:1 Liss Rhod PE lipid content of the GUVs. H) Excitation/emission: 488/525 nm, from the CNTP-6AF fluorophore. I) Ortholog z-stack overlay of the red and green channels with cross-sectional panels. Scale bars are 20  $\mu\text{m}$ .

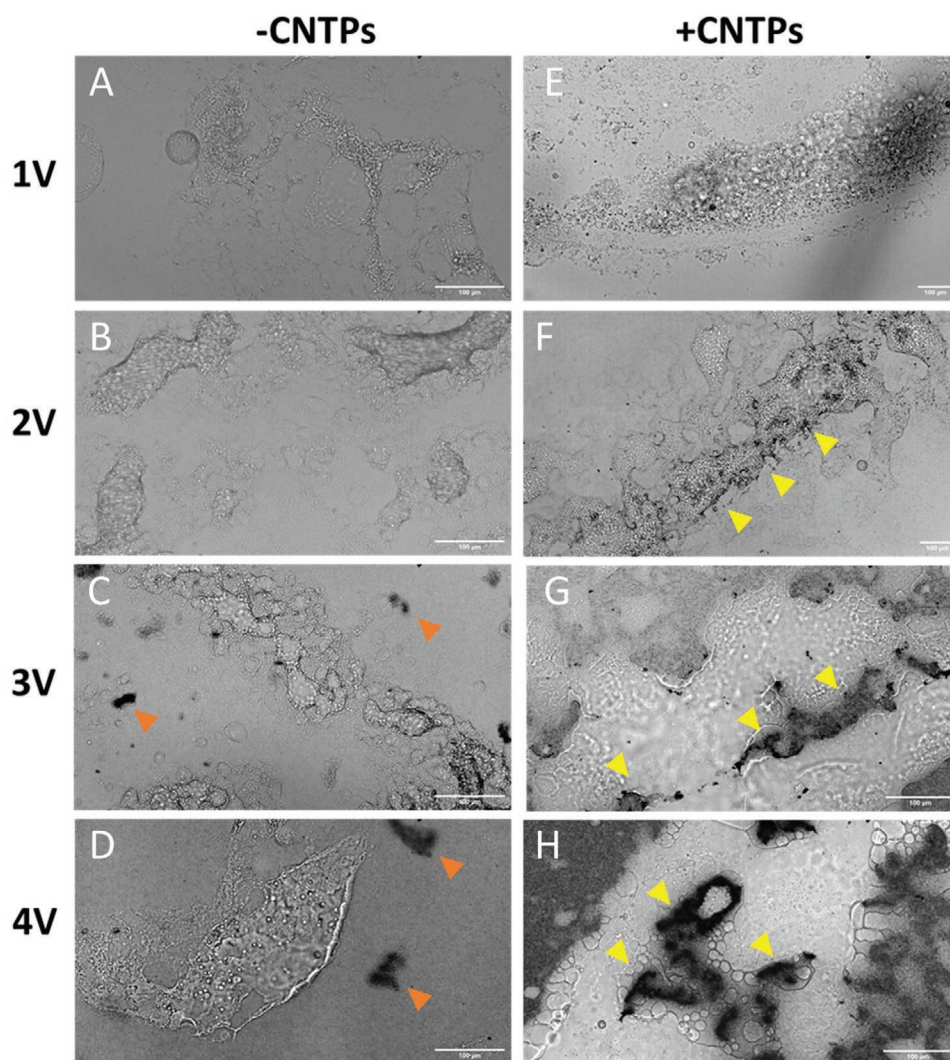


**Figure 3.** Brightfield images of GUVs with and without CNTPs incorporated and with varying DC voltages applied for 1 h. GUVs were rehydrated with 20  $\mu\text{L}$  water for 15 minutes before being immersed in 1 ml  $\text{HAuCl}_4$  (1 mM). Panels A, B, C and D are without CNTPs. Panels E, F, G and H are with CNTPs. A and E: 1 V, B and F: 2 V, C and G: 3 V, D and H: 4 V. Scale bars show 100  $\mu\text{m}$ . Yellow arrows indicate the supposed reduced gold aggregates formed after application of voltage and attached to the lipid surface. Orange arrows indicate large, reduced gold aggregates formed at the driving electrodes that have broken off and are floating in solution while yellow arrows indicate gold reduced at the lipid surface.

GUVs containing both the 18:1 liss rhodamine PE and the CNTP-6AF were imaged with fluorescence microscopy (Figure 2). These images show that the CNTPs are fully integrated within the GUV membrane with green fluorescence from the 6AF visible throughout the GUV population.

We used confocal microscopy imaging to investigate whether the CNTPs were integrated within the GUV outer membranes or whether they had been collected and pooled within the GUVs. A sample of GUVs imaged by confocal microscopy can be seen in Figure 2G–I. We observed halo type rings which define the GUV in the microscopy images (Figure 2G–I). These images show that CNTP-6AF molecules are localized to the outer membrane of the GUVs. This observation is also supported by the TEM images in Figure S3, Supporting Information.

To establish if we could use the CNTs as BPEs to facilitate membrane electron transfer we exposed the CNTPs-modified GUVs to an electric field, causing the CNTs to polarize. This

provides the thermodynamic driving force to facilitate redox reactions at the CNTPs without direct-wired contact to the feeder electrodes. In this experiment GUVs were submerged in a solution of 1 mM gold chloride ( $\text{HAuCl}_4$ ) between two driving electrodes and electrochemical reduction of gold (Equation (2)) was used as a tool to visualize the nano-BPEs activity. **Figure 3** shows brightfield images of GUVs (with and without CNTP incorporation) after the application of a direct current (DC) voltage for 1 h in the presence and absence of  $\text{HAuCl}_4$ . At higher voltages we observe that GUVs fuse.

In Figure 3 it can be seen that gold deposits become visible at GUVs modified with CNTPs after the application of 2 V for 1 h and become larger when increased voltage is applied. On application of 4 V for 1 h there is very little space left as it is occupied by the gold deposits. We then followed a time course of this process to further highlight the dynamic nature of the Au deposition process. Importantly, this only occurs on

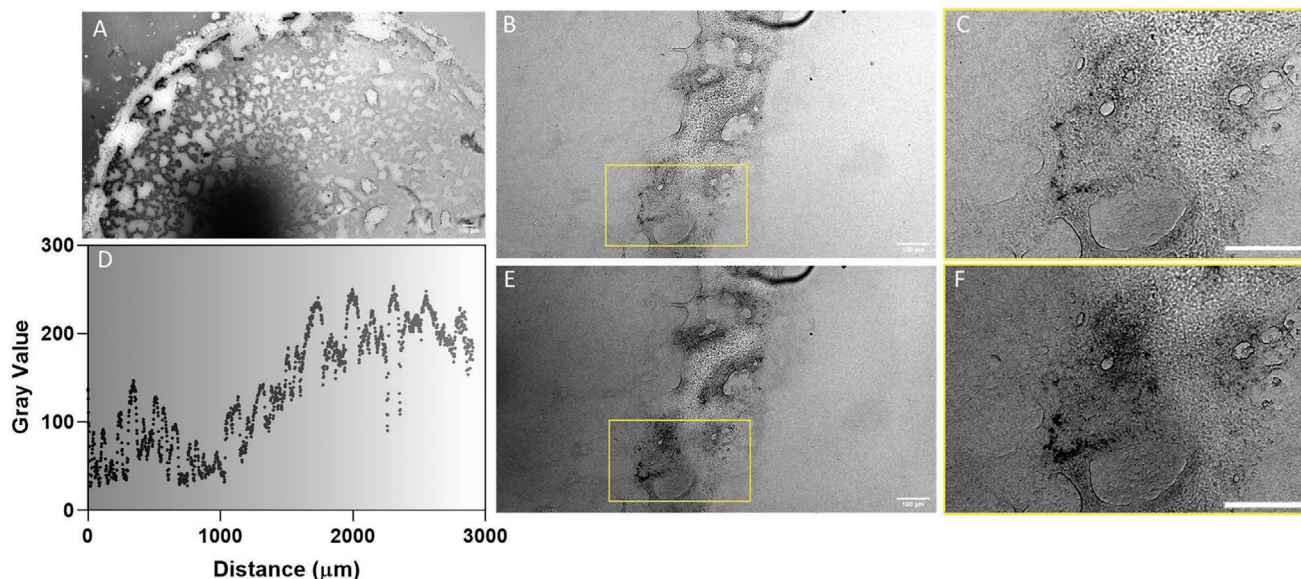


**Figure 4.** Brightfield images of GUVs with CNTPs incorporated. GUVs were rehydrated with 20  $\mu\text{L}$  water for 15 min before submission in 1 mL  $\text{AuCl}_4$  (1 mM). A DC of 4 V was applied. A) Lower magnification image showing the distribution of gold deposits across the GUV spot. Panels (B) and (C) are images taken 30 min after the beginning of stimulation. D) Gray scale values calculated by ImageJ when a line is drawn across (A). E, F) The same sample area imaged 45 min after the beginning of stimulation. Right-hand panels are enlarged regions of the areas indicated in the left-hand panels. All scale bars are 100  $\mu\text{m}$ .

the application of the voltage and in the presence of CNTPs. **Figure 4A** shows how the gold deposits were distributed across the whole GUV spot after 4 V had been applied. The gold deposits are opaque so while imaging with an inverted light microscope they appear black. We subsequently plotted the image intensity values across the GUV spot (**Figure 4D**) that shows that the gold is preferentially reduced at one end of the GUV spot with a concentration gradient formed across the sample. **Figure 4** shows snapshots of the lipids containing CNTPs at 30 min (**Figure 4B,C**) stimulation and 45 min stimulation (**Figure 4E,F**). The regions outlined highlight a specific region where the gold deposition growth can be seen. The CNTPs within the GUVs act as nucleation points for the electrochemically induced reduction and deposition. As time progresses with the application of a potential these deposits grow, as described in the literature,<sup>[30]</sup> and eventually break off allowing more gold reduction and deposits to grow. The gold deposition is evident at time points throughout the experiment (**Figure 4**) and is also seen in the time-lapse data of the gold aggregation (see **Figure S7**, Supporting Information).

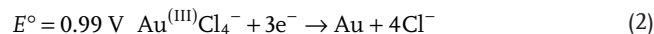
We used energy dispersive X-ray analysis (EDS) coupled with scanning electron microscopy (SEM) to further confirm gold deposition. Several different applied voltages were tested in samples made with and without CNTP incorporation as well as the original gold chloride solution. Multiple regions were randomly selected for imaging. To ensure the images were representative, multiple regions were analyzed for each sample. Elemental reconstructions of carbon, gold, and chlorine for the original gold chloride solution and a GUV sample exposed to voltage are shown in **Figure 5**.

The original solution of gold chloride shows that the gold and chlorine colocalize as expected in the absence of an applied voltage. After application of a potential to the sample with

GUVs containing CNTPs, concentrated deposits of gold appear with no corresponding chlorine detected. This observation supports the data from **Figures 3** and **4** and that the deposits visualized after application of voltage are indeed reduced gold.

Macro- and micro-sized BPEs obey the rule that only a fraction of the applied potential is experienced at the BPE terminus. This behavior is defined by Equation (1)<sup>[36]</sup> which explains the relationship between the potential at the BPE ( $\Delta E_{\text{elec}}$ ), the length of the BPE ( $l_{\text{elec}}$ ), the distance between the driving electrode ( $l_{\text{channel}}$ ), and the driving potential ( $E_{\text{tot}}$ ). If nano-BPEs obeyed the same rules, to reach a potential of at least 1 V (to (required to reduce the gold, see Equation (2)) we would need to be applying at least 3 V if we considered the entire GUV spot as a BPE, or 1.2 kV if we consider the CNTPs as individual BPEs. As clearly neither of these is the case, it is important to better understand the nature of nano-BPEs. Finding the threshold potential for the gold reduction at the CNTPs was, therefore, an important first step in understanding how they work.

$$\Delta E_{\text{elec}} = E_{\text{tot}} \left( \frac{l_{\text{elec}}}{l_{\text{channel}}} \right) \quad (1)$$



By applying voltages for 1 h at 0.1 V increments, it was discovered that gold was reduced at applied voltages as low as 1.5 V. Moreover, with this low voltage, the GUVs did not completely fuse as seen in **Figure 3**, and growths of gold deposits could be seen clearly at individual GUVs (see **Figure 6C**) with images showing the gold forming directly at the membrane of the GUV containing CNTPs. We wanted further evidence that wireless electrochemical deposition was occurring. Therefore, we monitored the signal from the 6-AF fluorophore attached to the

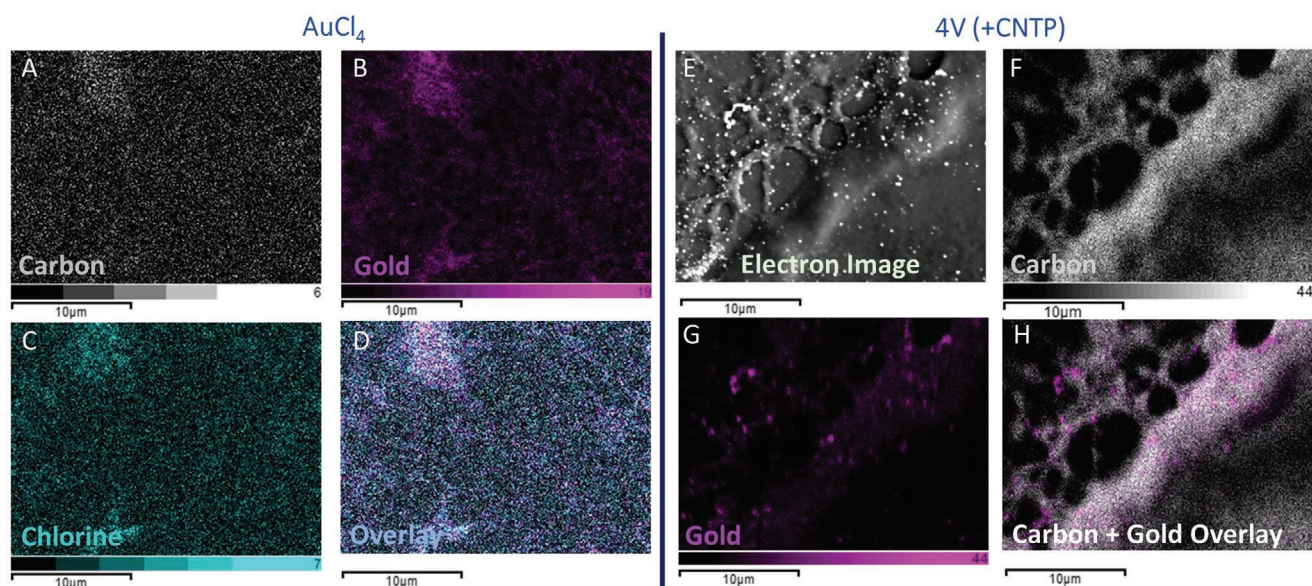


**Figure 5.** EDS analysis images. Panels A, B, C and D are from a sample of  $\text{AuCl}_4$  solution (1 mM) dried under vacuum on a glass coverslip. Panels E, F, G and H are from a sample of GUVs containing CNTPs on a glass coverslip, 4V (DC) applied for 1 hour in a solution of 1 mM  $\text{AuCl}_4$  then dried under vacuum. Carbon (A,D), gold (magenta colored, B,G) and chlorine (cyan colored, E) elements were mapped and overlays plotted (D,H). Intensity scale bars for each element are shown under each panel. Scale bars are 10  $\mu\text{m}$ .

CNTPs and observed changes in fluorescence by using optical microscopy on the application of a voltage. We observed that GUVs were polarized resulting in gold deposits at one end only that also quenched the CNTP fluorescence (see Figure 6D–F). This observation further supports that the gold was being electrochemically deposited at the CNTP tip.

We wanted to provide further mechanistic evidence to establish that direct bipolar electrochemical induced deposition of gold was occurring. To confirm that this deposition was not arising due to a mediated electrochemical process that was occurring due to electrochemically induced water splitting and radical formation that subsequently reduced the gold, we replaced the gold chloride solution with an equivalent solution of zinc chloride. This would establish if there was a potential relationship that would be indicative of the different standard potential of Zn ( $-0.76\text{ V}^{[37]}$ ) versus Au ( $+0.99\text{ V}^{[30]}$ ) (Figure S6, Supporting Information) while also confirming that low, cell-friendly voltages can be used with nano-BPEs for multiple, different redox reactions. If metal deposition was driven by radical formation during water splitting, then there would be no voltage difference observed with the applied feeder electrode potential. On the contrary, we observed that a significantly higher applied potential of 7 V at the feeder electrodes was required to observe reduced Zn (Figure S6, Supporting Information) versus the 1.5 V that produced gold deposits. This result confirmed that the electrochemical mechanism is via direct bipolar electrochemical induced deposition and not an indirect electrochemical method.

We then wanted to show that CNTPs could act as BPEs in the cell membrane of NG108 cells and that electron transfer across the membrane via CNTPs could be modulated on-demand using wireless electrochemistry. We first provide evidence that CNTPs could be inserted into the membrane. We found that incubation of the CNTPs with the cells for 4 h was

sufficient to allow CNTPs to self-insert into the cellular membrane (Figure 7F). This behavior is consistent with previous work that shows that lipid-coating the CNTPs allows them to self-insert within the lipid membrane.<sup>[38]</sup> A control set of cells just incubated with phosphate buffered saline (PBS) (see Figure 7B) showed similar changes in cellular morphology which we attribute to the CNTP insertion. On the addition of CNTPs to the cell, we wished to establish that the CNTPs did not affect cell viability. To assess viability after incubation with CNTPs in PBS buffer, cells were washed and the live cell stain NucBlue was added. Images of the cells after the CNTP addition show a substantial population of healthy cells (as indicated by the NucBlue fluorescent signal) left on the cell culture plate, with the viable cell percentage comparable to the PBS control. After incubation with either the PBS or CNTPs, cells were submerged (as before with the GUVs) in 1 mM  $\text{AuCl}_4$  (in MilliQ water) and were stimulated for 1 h at voltages between 1 and 4 V. Due to the presence of proteins such as native VDACS within the cell membrane and their ability to reduce molecules once activated by voltage, there was a small amount of reduced gold at the membrane surface in all control samples as well (Figure 7G). This made it difficult to tell at the lowest voltage of 1.5 V, if there were significantly more deposits on cells containing CNTPs which was occurring via bipolar electrochemistry. However, by 2 V there is a clear difference between the CNTP samples and the controls with deposits associated with the cell plasma membranes containing CNTPs (see Figure 7H).

Unlike the GUV samples which fused at higher voltages, the cells remain separated. Therefore, even if we hypothesized that the cell body was acting as a BPE rather than the individual CNTPs within its membrane, then according to Equation (1) we would need to be applying a driving potential of 800 V. As less than 2 V was required, this observation supports the

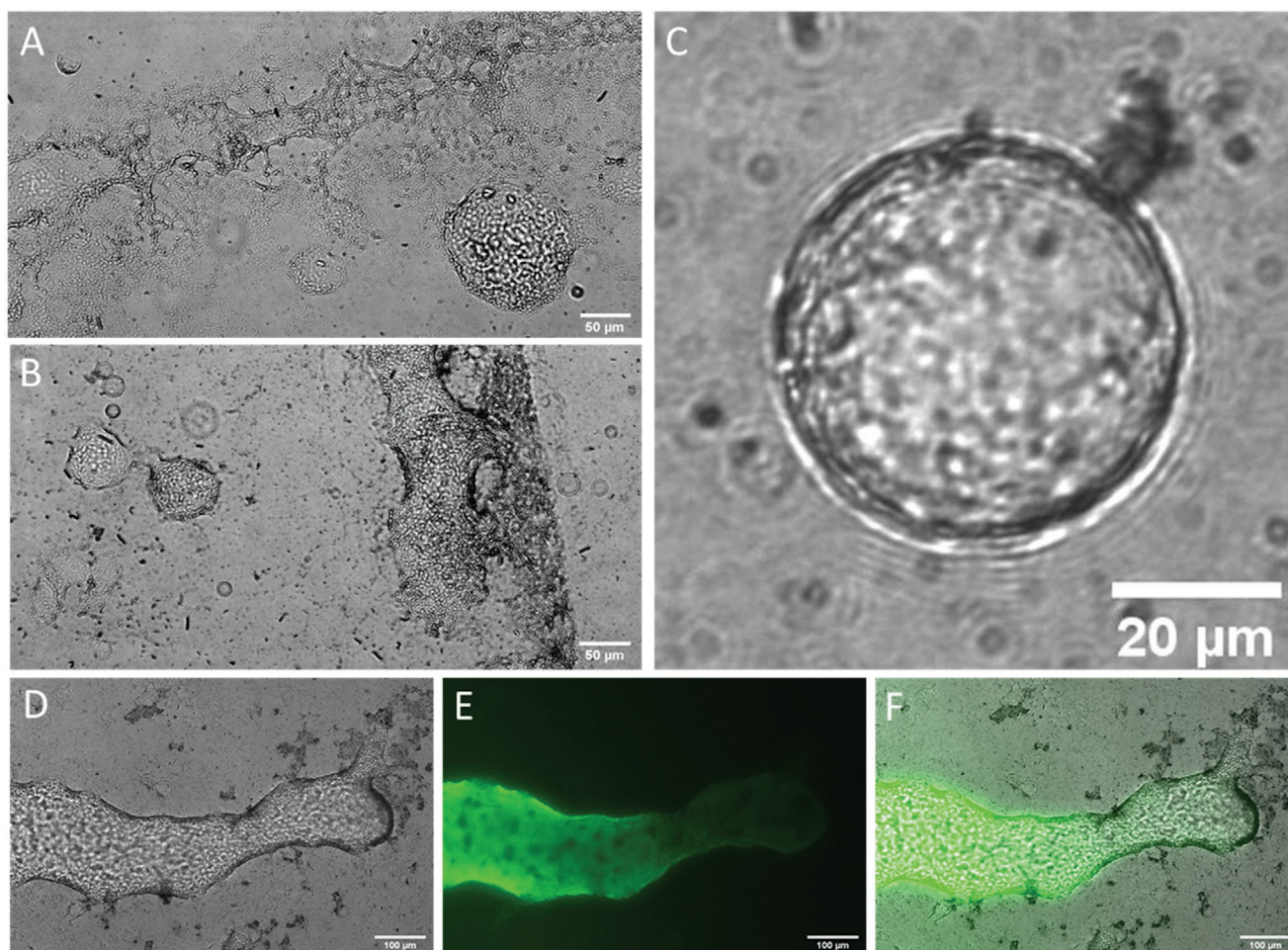


**Figure 6.** GUVs were stimulated with 1.5V DC for 1 h while submerged in 1 mM  $\text{AuCl}_4$  solution. A) GUVs without CNTPs. B) With CNTPs and C) a zoomed image of a single GUV containing CNTPs after 1.5 V application and visible gold deposition on the membrane. D–F) Show fused GUVs after application of 1.5 V for 1 h. D) Brightfield image showing gold deposits at the right hand end of the GUV; E) Fluorescence image from the CNTP-6AF and F) overlay image showing how the gold deposits quench the fluorescence. A,B) scale bars are 50  $\mu\text{m}$ , C) scale bar is 20  $\mu\text{m}$  and D–F) Scale bars are 100  $\mu\text{m}$  in length.

idea that the CNTPs are acting as individual nano-BPEs which do not follow the same rules as macro- and micro-BPEs. One reason why lower driving voltage is required at the nanoscale, especially, for electrodes with a radius below 50 nm, is that the diffuse double layer extending from the CNTPs BPEs into the solution becomes significant,<sup>[33]</sup> and dramatically increases the capacitance associated with the charging current and at the CNTPs. Our observation of lower voltages required to initiate wireless electrochemistry at the nanoscale are also supported by our previous work on nano-BPEs.<sup>[39]</sup>

We also performed finite element modeling to further aid our understanding of bipolar electrochemistry at a CNTP embedded within a GUV (Figure 8). The model was based on the CNTP-modified GUV with the CNTPs having a diameter of 0.8, 2, 5, and 10 nm with a permittivity of 100 (semiconducting tubes) or 2000 (metallic tubes) for CNTPs types, respectively,<sup>[40]</sup> in a solution of 1 mM  $\text{AuCl}_4^-$  and  $\text{H}^+$  as the ions with a diffusion coefficient for  $\text{H}^+$ :  $9.3 \times 10^{-9} \text{ m}^2 \text{ s}^{-1}$  and for  $\text{AuCl}_4^-$ :  $31.4 \times 10^{-12} \text{ m}^2 \text{ s}^{-1}$ . Calculated electric potential surface demonstrated that the applied potential propagated through

the CNTP-lipid (Figure 8A–C). We calculated the electric potential distribution along the CNTP walls (Figure 8D) and extracted the potential value at the position near the CNTP tips (Figure 8E). The results demonstrated that there is a significant difference in the voltage density at the tip of the electrode at different diameter length scales. There is approximately a 30% increase in the induced voltage density at the pole on the CNTP when comparing the 1 nm diameter CNTPs to the 10 nm ones. This relationship in size in combination with the observation made by Compton et al.<sup>[33]</sup> explains why we are observing the electric field induced membrane electron transfers at potentials lower than predicted. This also indicates that the theory on bipolar electrochemistry at the nanoscale needs to be modified to take account of the enhanced voltage gradient observed at the nanoscale which facilitated bipolar electrochemistry at the nanoscale.

Even in light of these observations more work is needed to understand the exact relationship of capacitance at the nanoscale of BPEs in biology which we have begun to address.<sup>[41]</sup> However, we do show that nano-BPEs could be

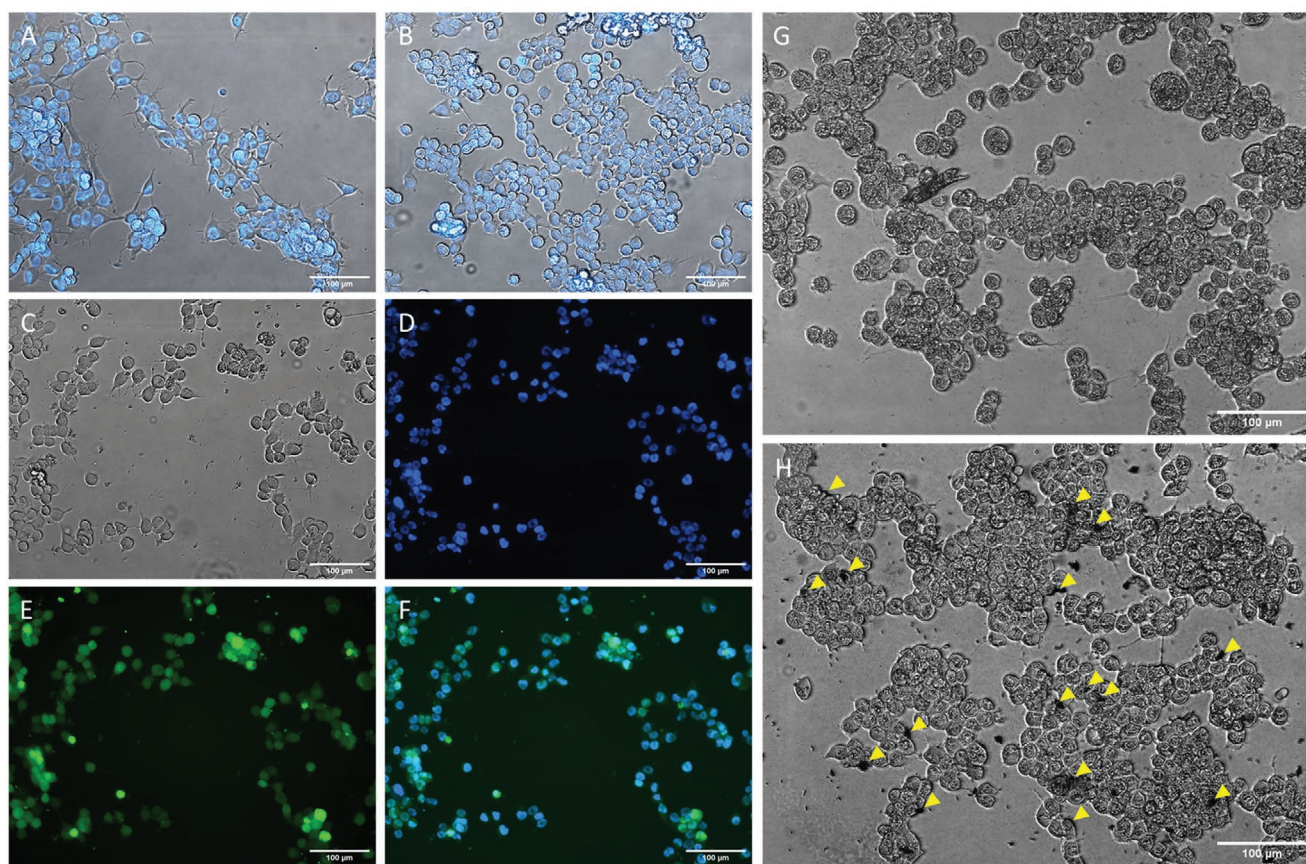


**Figure 7.** Wireless studies using NG108-15 cells. A) Cells before treatment with NucBlue stain (excitation/emission 360/460 nm). B) Cells after 4 h submerged in PBS with NucBlue stain. C–F) Cells after 4 h of CNTP-6AF treatment; C) optical image, D) Nucblue fluorescent image, E) CNTP-6AF fluorescence (excitation/emission 490/520 nm), F) the composite image of (D) and (E). G) Cells incubated with PBS for 4 h then subjected to 2 V, DC, for 1 h in 1 mM HAuCl<sub>4</sub> solution. H) Cells incubated with CNTPs for 4 h then subjected to 2 V, DC, for 1 h in 1 mM HAuCl<sub>4</sub> solution. Yellow arrows indicate reduced gold deposits associated with the cellular membrane. All scale bars are 100 μm.

polarized at low, biocompatible voltages and we could modulate electron transfer across biological membranes and effect a change on membrane potential.

### 3. Conclusion

Here, we have shown that CNTPs inserted and retained within lipids and plasma membranes of live cells where they can act as nano-BPEs. Despite their short size, the CNTPs can be polarized at low voltages (less than 2 V) shown by the reduction of gold chloride to gold at the surface of the lipids and plasma membrane. This observation was confirmed by both conventional microscopy and SEM–EDS analysis. We observe similar gold reduction on the CNTP BPEs inserted into membranes of live cells, where the reduction of gold chloride was visible at 2 V applied potential. Such low, cell-friendly, voltages have only recently been theorized and shown and are unique to nano-BPEs with much larger voltages required for both micro- and macro-sized BPEs. Our observations open up the potential to use nano-BPEs in electronic therapeutics and in their development to help treat neurodegenerative diseases and cancer as artificial VDACS and TPMET mimics.

### 4. Experimental Section

**Materials:** All materials unless otherwise stated were purchased from Sigma-Aldrich. Solutions of HAuCl<sub>4</sub> were made up to 1 mM in MilliQ water.

**Carbon Nanotube Porin Synthesis:** The synthesis of CNTPs was described in depth previously.<sup>[25]</sup> Briefly, 0.5 mg single-walled CNTs were baked incrementally starting at 100 °C and increasing temperature by 20 °C every 2 min until a temperature of 475 °C was reached. 28 mg 1,2-dioleoyl-sn-glycero-3-phosphocholine (DOPC, Avanti Polar Lipids) was dried within a scintillation vial (VWR) using a RotaVapor Evaporator (Buchi). The baked CNTs were then solubilized with the dried DOPC with 14 mL MilliQ water. The solution was placed in a sonicator water bath (Branson 1800) for ≈30 min to fully solubilize the CNTs. The solution was then transferred to the ultrasonicator (QSonica) within a sound enclosure (QSonica) with a microtip diameter of 0.25 inches. The sample was held by a custom-made sample holder that allowed water circulation that was kept at a constant temperature of 30 °C by a recirculating chiller (Polyscience). The sample was sonicated for a total of 16 h by pulses (3 s on, 1 s off) at an amplitude of 35%. After sonication, the sample was centrifuged (Beckman Coulter with Allegra X-Rotor) for 1 h at 10 300 × g. The supernatant containing the CNTPs was then carefully aspirated for further use. Calculation of yield of CNTPs was measured as the number of CNTPs per vesicle via a proton assay and is described in depth here.<sup>[25]</sup>

**Carbon Nanotube Porin Modification and Purification:** A concentration of ≈20 CNTPs/vesicle/mL was dried in glass vials using a CentriVap



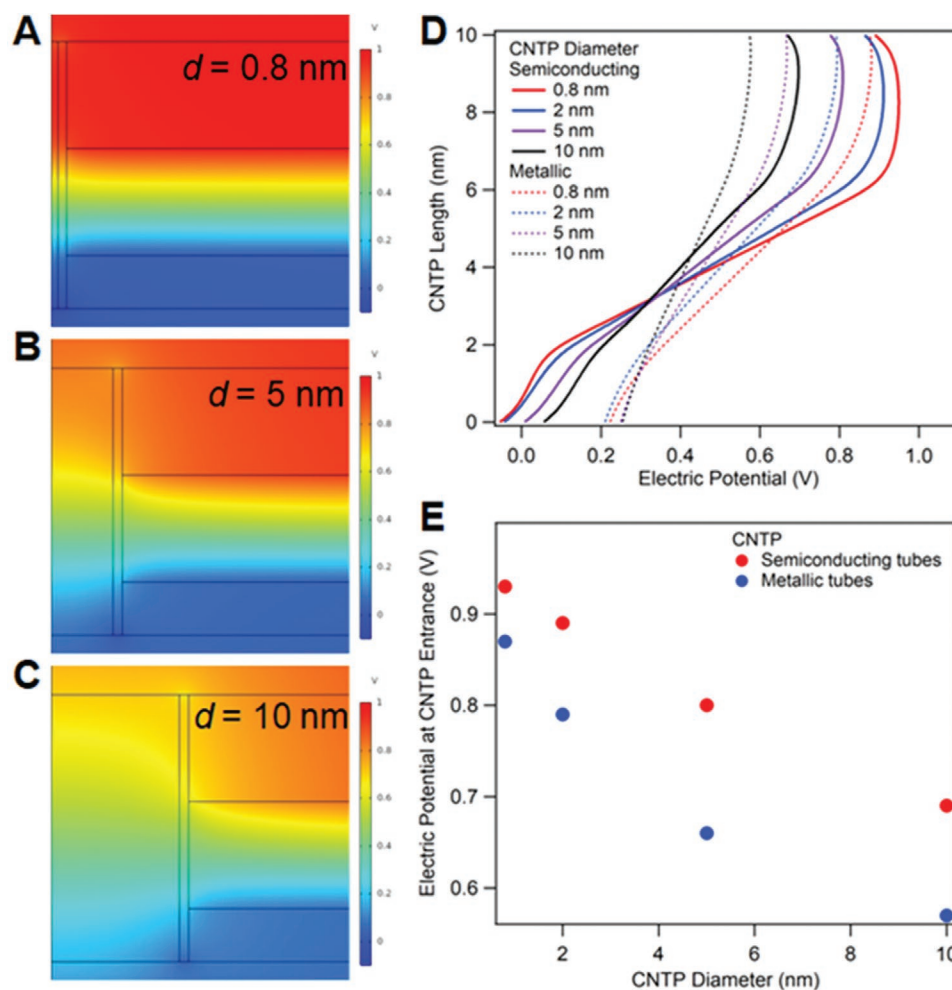


**Figure 8.** A–C) Modeled electric potential presented by electric potential surface (A–C) and the distribution along the carbon nanotube porin (CNTP) walls (D), and E) electric potential values at the entrance when comparing CNTP diameters and electrical properties.

micro-IR concentrator (Labconco). The dried CNTPs were then resolubilized in 1 mL MilliQ water containing 80 mM EDC and 20 mM NHS and left at room temperature for 30 min. A saturated solution ( $\approx 25$  mM) of 6AF was made in a solution mix of ethanol and water (50:50) and spun for 1 min on a benchtop centrifuge to remove particulates. 100  $\mu$ L of the 6AF solution was added to the CNTPs giving a final concentration of  $\approx 2.5$  mM. This solution was mixed gently by pipetting and then allowed to react overnight at room temperature in the dark. The next day the bound CNTP-6AF was separated from unbound components by gel chromatography using a sepharose CL-6B column. Fractions were collected in a 96 well plate (Costar) and absorbance was measured in a Microplate reader (SpectraMax iD3 Multi-mode Microplate reader) at 1000 nm to detect CNTPs and 495 nm to detect 6AF. Selected fractions were then pooled and stored at 4  $^{\circ}$ C until use.

**Giant Unilamellar Vesicle Formation:** GUVs were formed using an adaptation of methods published previously by Orwar et al.<sup>[42]</sup> and Manley and Gordon.<sup>[43]</sup> Lipids were dried within scintillation vials (VWR) containing 2 mg DOPC and 0.02 mg 1,2-dioleoyl-sn-glycero-3-phosphoethanolamine-N-(lissamine rhodamine B sulfonyl) (18:1 Liss Rhod PE, Avanti Polar Lipids) with a RotaVapor Evaporator (Buchi). The lipids were rehydrated with 1 mL of CNTP-6AF (or 1 mL water) and solubilized briefly in a water bath sonicator (Fisher Brand FB11021) before being left at room temperature for 30 min to form large unilamellar vesicles (LUVs). The LUV solution went through a process of freeze/thaw

ten times using liquid nitrogen (BOC) to freeze and a water bath on a hot plate (VWR) set at 100  $^{\circ}$ C to thaw the solution. This was done to break down double membranes produced when the LUVs were forming.

Glass coverslips (13 mm diameter, VWR) were cleaned by briefly sonicating (Fisher Brand FB11021) in acetone for 30 s followed by isopropanol for 10 s and rinsing with MilliQ water. Cleaned coverslips were dried with nitrogen gas. 5  $\mu$ L LUVs were pipetted onto the center of coverslips and dried under vacuum. Once dried coverslips were placed within a 12 well plate and rehydrated with 20  $\mu$ L for at least 10 min to allow the GUVs to form.

**Wireless Electrochemistry:** Wireless electrochemical experiments were conducted within a 24 well plate (Costar) with a custom-made (LLNL) well insert that could hold the driving electrodes at a set position and distance apart. Hypodermic needles were used as driving electrodes (25G, BD Microlance) and held in place by the insert. Dried LUVs were rehydrated to form GUVs for at least 10 min before electrical stimulation by the power source (Programmable AC/DC Power Source EC1000SA, NF Corporation). A DC was used in all cases with the voltage applied varying between 1 and 4 V and applied to the samples for 1 h.

**Fluorescence Microscopy:** Images were captured with a Nikon fluorescent microscope (Model: TI-DH) with an optiMOS sCMOS camera and utilizing NIS-Elements (version 4.60) software.

**Confocal Microscopy:** Confocal microscopy was conducted using a Zeiss LSM 880 on a Zeiss Axio Observer platform system running Zen Black software. Z-stacks were imaged with a Plan-Apochromat 20 $\times$ /0.8

M27 objective with a 1  $\mu\text{m}$  depth per slice analysis performed to a depth of 20.35  $\mu\text{m}$ . The pinhole was set to 0.73 AU (for an excitation wavelength of 561 nm) and 0.87 AU (for an excitation wavelength of 488 nm). The scanning was in unidirectional sequential line mode with four times averaging to reduce noise. Images were analyzed with a combination of ImageJ and Zen Blue.

**Scanning Electron Microscopy–Electron Dispersive X-Ray Analysis:** Back-scattered electron images and energy-dispersive X-ray spectroscopy (EDS) element maps were collected using a JEOL JSM-6490LV SEM with Oxford Instruments X-MAX INCA EDS system. The SEM was set to an accelerating voltage of 10 kV and a specimen chamber pressure of 15 Pa. Specimen regions with relatively high concentrations of carbon and gold were selected by mapping at low magnification; then rectangular areas 26  $\mu\text{m}$  by 20  $\mu\text{m}$  in size were mapped with a step size of 0.1  $\mu\text{m}$ . The X-ray energy window for the Au  $M\alpha$  line was adjusted to reduce overlap with the P K line.

**Cell Culture:** NG108-15 cells (ECACC) were cultured in Dulbecco's modified media (Gibco) supplemented with 10% FBS and 1% penicillin streptomycin. Cells were seeded in a 24 well plate (Costar, tissue culture treated) at 50 000 cells/mL and grown for 2 days to reach confluency at 37 °C and 5%  $\text{CO}_2$ . When confluent, media was carefully aspirated from wells by pipetting and replaced with either 0.5 mL PBS or modified CNTPs (CNTP-6AF) and returned to the incubator for 4 h. After 4 h, the solution was replaced with 1 mM  $\text{HAuCl}_4$  (in ultrapure MilliQ water) and wireless experiments were conducted as described previously.

**Modeling:** To explore the applied electric potential on the CNTP, this system was modeled in the finite element analysis software COMSOL Multiphysics 5.5. The authors' simulation used two physical modules for describing the electric potential and the  $\text{AuCl}_4^-$  distribution in this system: electrostatic and transport of diluted species. In this simplified model, the authors set up an axisymmetric cell that had two reservoirs with 50 nm in radius and height. These chambers were separated by lipid bilayers, which were 4 nm in thickness, and with a CNTP channel placed in the center. The external potential was applied at the upper boundary of the top reservoir and the bottom reservoir was grounded. 1 V was the voltage applied in this model system. The length of CNTP was 10 nm, and the thickness of the CNTP wall was 0.34 nm. The tips of CNTPs were assigned with a charge density equal to four electrons. 1 mM  $\text{AuCl}_4^-$  was the starting concentration for both reservoirs. The CNTP carbon-to-carbon diameters,  $d$ , with 0.8, 2, 5, and 10 nm were varied to probe the effect of tip size on electric potential distribution. The relative permittivity of CNTP was also altered using two values: 100 and 2000, which corresponded to semiconducting tubes and metallic tubes, respectively.

## Supporting Information

Supporting Information is available from the Wiley Online Library or from the author.

## Acknowledgements

This work was supported by the Engineering and Physical Sciences Research Council (Grant numbers EP/R004072/1, EP/L022494/1). Parts of this work (CNTP fabrication and characterization by YCY, SB, and AN) were performed at the Lawrence Livermore National Laboratory under the auspices of the US Department of Energy under Contract DE-AC52-07NA27344, and were supported by the US Department of Energy, Office of Basic Energy Sciences, Division of Materials Sciences and Engineering under Award SCW0972.

## Conflict of Interest

The authors declare no conflict of interest.

## Data Availability Statement

Data can be found at <https://doi.org/10.17639/nott.7118>.

## Keywords

bipolar electrochemistry, carbon nanotube porins, cell electrochemistry, membrane potential, trans-plasma membrane electron transport systems, voltage-dependent anion-selective channels

Received: April 28, 2021

Revised: May 27, 2021

Published online:

- [1] D. D. Principe, L. Avigliano, I. Savini, M. V. Catani, *Antioxid. Redox Signaling* **2011**, *14*, 2289.
- [2] a) H. Fischer, *Antioxid. Redox Signaling* **2009**, *11*, 2453; b) A. Eccardt, T. Bell, L. Mattathil, R. Prasad, S. Kelly, J. Fisher, *Antioxidants* **2017**, *6*, 89.
- [3] J. Ly, A. Lawen, *Redox Rep.* **2003**, *8*, 3.
- [4] D. Sarr, E. Tóth, A. Gingerich, B. Rada, *J. Microbiol.* **2018**, *56*, 373.
- [5] D. J. Lane, A. Lawen, *Biofactors* **2009**, *34*, 191.
- [6] a) M. Block, *BMC Neurosci.* **2008**, *9*, 1471; b) A. Jana, K. Pahan, *J. Biol. Chem.* **2004**, *279*, 51451.
- [7] A. Bruce-Keller, S. Gupta, T. Parrino, A. Knight, P. Ebenezer, A. Weidner, H. LeVine, J. Keller, W. Markesbery, *Antioxid. Redox Signaling* **2010**, *12*, 1371.
- [8] A. J. Robinson, A. Jain, H. G. Sherman, R. J. M. Hague, R. Rahman, P. Sanjuan-Alberte, F. J. Rawson, *Adv. Ther.* **2021**, *4*, 2000248.
- [9] S. Gibney, J. M. Hicks, A. Robinson, A. Jain, P. Sanjuan-Alberte, F. J. Rawson, *Wiley Interdiscip. Rev.: Nanomed. Nanobiotechnol.* **2021**, *13*, e1693.
- [10] F. Elinder, N. Akanda, R. Tofighi, S. Shimizu, Y. Tsujimoto, S. Orrenius, S. Ceccatelli, *Cell Death Differ.* **2005**, *12*, 1134.
- [11] R. Marin, C. Ramírez, M. González, E. González-Muñoz, A. Zorzano, M. Camps, R. Alonso, M. Díaz, *Mol. Membr. Biol.* **2007**, *24*, 148.
- [12] a) W. Yu, M. Forte, *J. Bioenerg. Biomembr.* **1996**, *28*, 93; b) C. Mannella, *J. Bioenerg. Biomembr.* **1997**, *29*, 525.
- [13] S. Okada, W. O'Neal, P. Huang, R. Nicholas, L. Ostrowski, W. Craigen, E. Lazarowski, R. Boucher, *J. Gen. Physiol.* **2004**, *124*, 513.
- [14] H. Sherman, C. Jovanovic, A. Abuawad, D. Kim, H. Collins, J. Dixon, R. Cavanagh, R. Markus, S. Stolnik, F. Rawson, *Biochim. Biophys. Acta, Bioenerg.* **2019**, *1860*, 628.
- [15] a) L. Stockwin, J. Blonder, M. Bumke, D. Lucas, K. Chan, T. Conrads, H. Issaq, T. Veenstra, D. Newton, S. Rybak, *J. Proteome Res.* **2006**, *5*, 2996; b) L. Ning, B. Pan, Y. Zhao, Q. Liao, T. Zhang, G. Chen, W. Wang, Y. Yang, *Chin. J. Surg.* **2007**, *45*, 34.
- [16] N. Akanda, R. Tofighi, J. Brask, C. Tamm, F. Elinder, S. Ceccatelli, *Cell Cycle* **2008**, *7*, 3225.
- [17] A. Grupi, I. Ashur, N. Degani-Katzav, S. Yudovich, Z. Shapira, A. Marzouq, L. Morgenstein, Y. Mandel, S. Weiss, *Small* **2019**, *15*, 1903006.
- [18] a) L. Fenno, O. Yizhar, K. Deisseroth, *Annu. Rev. Neurosci.* **2011**, *34*, 389; b) S. M. Spangler, M. R. Bruchas, *Curr. Opin. Pharmacol.* **2017**, *32*, 56.
- [19] a) D. T. Simon, E. O. Gabrielsson, K. Tybrandt, M. Berggren, *Chem. Rev.* **2016**, *116*, 13009; b) S. Löffler, B. Libberton, A. Richter-Dahlfors, *Electronics* **2015**, *4*, 879; c) K. Famm, B. Litt, K. J. Tracey, E. S. Boyden, M. Slaoui, *Nature* **2013**, *496*, 159.

- [20] Y. Ma, J. Bao, Y. Zhang, Z. Li, X. Zhou, C. Wan, L. Huang, Y. Zhao, G. Han, T. Xue, *Cell* **2019**, *177*, 243.
- [21] a) M. Sushnitha, M. Evangelopoulos, E. Tasciotti, F. Taraballi, *Front. Bioeng. Biotechnol.* **2020**, *8*, 627; b) P. Nednoor, V. G. Gavalas, N. Chopra, B. J. Hinds, L. G. Bachas, *J. Mater. Chem.* **2007**, *18*, 1755; c) R. García-Fandiño, M. S. P. Sansom, *Proc. Natl. Acad. Sci. U. S. A.* **2012**, *109*, 6939.
- [22] a) A. K. Gupta, R. R. Naregalkar, V. D. Vaidya, M. Gupta, *Nanomedicine* **2007**, *2*, 23; b) J. Weingart, P. Vabbilisetty, X. L. Sun, *Adv. Colloid Interface Sci.* **2013**, *197–198*, 68.
- [23] K. Park, Y. Kuo, V. Shvadchak, A. Ingargiola, X. Dai, L. Hsiung, W. Kim, H. Zhou, P. Zou, A. Levine, J. Li, S. Weiss, *Sci. Adv.* **2018**, *4*, e1601453.
- [24] P. Rothmund, *Nature* **2006**, *440*, 297.
- [25] R. H. Tunuguntla, A. Escalada, V. A. Frolov, A. Noy, *Nat. Protoc.* **2016**, *11*, 2029.
- [26] T. Hodge, M. Colombini, *J. Membr. Biol.* **1997**, *157*, 271.
- [27] a) Y. Li, Z. Li, F. Aydin, J. Quan, X. Chen, Y.-C. Yao, C. Zhan, Y. Chen, T. A. Pham, A. Noy, *Sci. Adv.* **2020**, *6*, eaba9966; b) J. R. Sanborn, X. Chen, Y.-C. Yao, J. A. Hammons, R. H. Tunuguntla, Y. Zhang, C. C. Newcomb, J. A. Soltis, J. J. De Yoreo, A. Van Buuren, A. N. Parikh, A. Noy, *Adv. Mater.* **2018**, *30*, 1803355.
- [28] J. Z. Wang, Z. Q. Ding, F. Zhang, W. B. Ye, *Mater. Sci. Eng., C* **2017**, *77*, 1247.
- [29] L. Koefoed, S. Pedersen, K. Daasbjerg, *Curr. Opin. Electrochem.* **2017**, *2*, 13.
- [30] C. Warakulwit, T. Nguyen, J. Majimel, M. H. Delville, V. Lapeyre, P. Garrigue, V. Ravaine, J. Limtrakul, A. Kuhn, *Nano Lett.* **2008**, *8*, 500.
- [31] N. Karimian, P. Hasemi, A. Afkhami, H. Bagheri, *Curr. Opin. Electrochem.* **2019**, *17*, 30.
- [32] a) Q. Guo, C. Lei, W. Chen, J. Zhang, B. Huang, *Cell Rep. Phys. Sci.* **2021**, *2*, 100299; b) R. Hao, Y. Fan, C. Han, B. Zhang, *Anal. Chem.* **2017**, *89*, 12652; c) K. Ino, R. Yaegaki, K. Hiramoto, Y. Nashimoto, H. Shiku, *ACS Sens.* **2020**, *5*, 740.
- [33] E. Dickinson, R. Compton, *J. Phys. Chem. C* **2009**, *113*, 17585.
- [34] S. F. Fenz, K. Sengupta, *Integr. Biol.* **2012**, *4*, 982.
- [35] T. Baumgart, A. T. Hammond, P. Sengupta, S. T. Hess, D. A. Holowka, B. A. Baird, W. W. Webb, *Proc. Natl. Acad. Sci. USA* **2007**, *104*, 3165.
- [36] a) J. Duval, J. Kleijn, H. Leeuwen, *J. Electroanal. Chem.* **2001**, *505*, 1; b) J. F. L. D. and, H. P. v. Leeuwen, J. Cecilia, J. Galceran, *J. Phys. Chem. B* **2003**, *107*, 6782; c) J. F. L. Duval, M. Minor, a. J. Cecilia, H. P. v. Leeuwen, *J. Phys. Chem. B* **2003**, *107*, 4143.
- [37] Standard Reduction Potential, <https://chem.libretexts.org/@go/page/282> (accessed: March 2021).
- [38] J. Geng, K. Kim, J. Zhang, A. Escalada, R. Tunuguntla, L. R. Comolli, F. I. Allen, A. V. Shnyrova, K. R. Cho, D. Munoz, Y. M. Wang, C. P. Grigoropoulos, C. M. Ajo-Franklin, V. A. Frolov, A. Noy, *Nature* **2014**, *514*, 612.
- [39] P. Sanjuan-Alberte, A. Jain, A. Shaw, S. Abayzeed, R. Dominguez, M. Alea-Reyes, M. Clark, M. Alexander, R. Hague, L. Perez-Garcia, F. Rawson, *ACS Appl. Nano Mater.* **2019**, *2*, 6397.
- [40] W. Lu, D. Wang, L. Chen, *Nano Lett.* **2007**, *7*, 2729.
- [41] A. Robinson, A. Jain, R. Rahman, S. Abayzeed, R. Hague, F. Rawson, *ChemRxiv* **2020**, [https://chemrxiv.org/articles/preprint/Impedimetric\\_Characterization\\_of\\_Bioelectronic\\_Nano-Antennae/12601883](https://chemrxiv.org/articles/preprint/Impedimetric_Characterization_of_Bioelectronic_Nano-Antennae/12601883).
- [42] A. Jesorka, N. Stepanyants, H. Zhang, B. Ortmen, B. Hakonen, O. Orwar, *Nat. Protoc.* **2011**, *6*, 791.
- [43] S. Manley, V. D. Gordon, *Curr. Protoc. Cell Biol.* **2008**, *40*, 24.3.1.